SPACE-TIME-POLARIZATION OPTICAL IMAGING THROUGH CLOUDS

Akira Ishimaru
Sermsak Jaruwatanadilok
Yasuo Kuga

Department of Electrical Engineering, Box 352500, University of Washington, Seattle, Washington 98195
Phone: 206-543-2169, Fax: 206-543-3842, E-mail: ishimaru@ee.washington.edu

ABSTRACT

This paper first discusses the optical scattering characteristics of clouds including water droplets and ice crystals. We then present the time-dependent vector radiative transfer theory making use of the Stokes vector, Mueller matrix and extinction matrix. In particular, we discuss the advantages of circular polarization over linear polarization. Next, we present imaging formulations including PSF, MTF and contrast and their generalizations to include the time and polarization characteristics. Examples are taken from optical imaging through clouds and include comparisons with imaging through turbulence. Improved image resolution techniques such as the polarization differential techniques are presented focusing on the behavior of ballistic and minimally scattered waves.

1. INTRODUCTION

In recent years, there has been renewed interest in optical imaging through scattering media. Optical imagery has several advantages: it has higher resolution than radar system, it can operate passively, it is noninvasive, and it is not as subject to jamming. It's disadvantages are that optical beams scatter and diffuse in media such as clouds, and it is necessary to identify and mitigate the effects of scattering on imaging. This paper first discusses the optical scattering characteristics of clouds, including spherical water droplets such as those in fog and cumulus clouds, and non-spherical ice crystals such as those in cirrus clouds. The propagation and scattering characteristics of optical beams are expressed in radiative transfer theory. A simplest approximation is the scalar radiative transfer theory with scalar phase functions such as the Henyey-Greenstein formula and its small-angle approximation. However, recent studies have identified the use of polarization and pulse characteristics for improved resolution. We present an overview of the time-dependent vector radiative transfer theory that makes use of the Stokes vector formulations, including the Mueller matrix and extinction matrix. In particular, we discuss the advantage of circular polarization (CP) over linear polarization (LP), as CP maintains its coherence for a much longer distance than LP, thus giving higher image resolution. We present our recent numerical studies on CP and LP propagation. It has been pointed out that the ballistic and minimally scattered waves can be used for improved resolution if we can separate them from the diffusive components. We discuss several techniques, including the use of polarization, time, and angular scattering with numerical examples. The quality of the imaging in terms of the transfer of the spatial spectrum through the medium can be expressed by Modulation Transfer Function (MTF). Generalization of conventional MTF to include the time and polarization is presented with numerical examples to show the improvement of image resolution resulting from the polarization and pulse studies. Imaging formulations are discussed in terms of MTF, Point Spread Function (PSF), contrast, Degree of Polarization (DOP), and Cross-Polarization Discrimination (XPD). Both CW and pulse scattering are discussed including Co-Polarization (Co-Pol), Cross-polarization (X-Pol), Coherent and incoherent components. Polarization differential technique is discussed showing one of the methods to improve the image resolution.

2. OPTICAL SCATTERING CHARACTERISTICS OF CLOUDS

2.1 Refractive Index of Water and Ice

Fog and cumulus clouds consist of spherical water droplets while cirrus clouds are mostly ice crystals of hexagonal shape. Refractive indices $(n' + in'')$ of water (at 10°c) and ice are shown in Fig. 1 and Table 1 [1],[2]. Note that the imaginary part n'' reaches minimum at $\lambda = 0.48\mu m$, but increases substantially as λ increases. The refractive indices of water and ice for $\lambda = 0.25$ to $2.5\mu m$ are shown in Fig. 2 [3]. They are similar in this range of wavelengths.

2.2 Optical properties of fog and clouds

Fog and cumulus clouds consist of spherical water droplets. Their median diameters are typically 0.5 to 10 μm. The number density may vary from 10^6 to 10^9 m^{-3} with typical value of 10^8 m^{-3}. Typical liquid content may vary from 0.03 to 2 g/m^3. The mean free path, also called "optical visibility" may be typically a few *km* to 50 *m*. Fig. 3 shows scattering pattern of fog particles at $\lambda = 0.5\mu m$ and $\lambda = 15\mu m$. Note that at $\lambda = 0.5\mu m$, there is a sharp peak in the forward direction, indicating that minimally scattered wave (snake wave) is important when the particle sizes are much greater than a wavelength. The scattering pattern of the size-distributed particles is often approximated by Henyey-Greenstein formula:

$$p(\mu) = \frac{W_o(1-g^2)}{\left[1+g^2-2g\mu\right]^{3/2}} \tag{1}$$

where W_o = albedo (ratio of scattering to total coefficient), g = anisotropy factor (mean cosine), $\mu = \cos\theta$
This can also be generalized to

$$p(s) = \frac{p(0)}{\left[1+\left(\frac{s}{s_o}\right)^2\right]^{n/2}} \tag{2}$$

where $s = 2\sin\frac{\theta}{2}$, s_o is constant representing the beam width, and n = spectral index. Note that n =3 represents Henyey-Greenstein with $s_o^2 = (1-g)^2 / g$, and n = 4 represents exponential correlation function, and n = 11/3 is for spectral density of turbulence. Table 2 shows and example of parameters for 1 *km* fog layers. Cirrus clouds consist of ice crystals of hexagonal complex structure with long sizes ranging from 15 to 700 μm. The concentration is approximately 3x10^6 m^{-3} and optical visibility is 12 *m* to 1 k*m* [4].

3. TIME-DEPENDENT VECTOR RADIATIVE TRANSFER

The vector radiative transfer equation for CW case was obtained previously [5],[6]. This is generalized to the time-dependent radiative transfer [7] for spherical particles. Consider narrow-band, time-dependent vector radiative transfer equations in a plane-parallel medium over the optical distance domain τ defined by $\tau = \rho\sigma_t z$ where ρ is the number density, σ_t is the total cross section of a single particle, and z is the actual distance as shown in Fig. 4. Note that τ_o is the optical depth defined by $\tau_o = \rho\sigma_t L$ where L is length of the slab of the random medium. Consider that the input is a delta function in time. The frequency-dependent vector raditive transfer equation for diffused component in frequency domain is given by the following

$$\mu\frac{\partial}{\partial\tau}\mathbf{I}_d(\omega,\tau,\mu,\phi) + \left(1+(\mu-1)i\frac{\omega}{\tau_o}\right)\mathbf{I}_d(\omega,\tau,\mu,\phi) = \int_0^{2\pi}\int_{-1}^{1}\mathbf{S}(\mu,\phi,\mu',\phi')\mathbf{I}_d(\omega,\tau,\mu',\phi')d\mu'd\phi' + \mathbf{F_o}(\tau,\mu,\phi)\exp(-\tau) \quad \text{for } 0 \le \tau \le \tau_o \tag{3}$$

The boundary conditions of 4 by 1 vector $\mathbf{I}_d$ are

$$\mathbf{I}_d(\tau=0) = 0 \quad \text{for } 0 \le \mu \le 1$$
$$\mathbf{I}_d(\tau=\tau_o) = 0 \quad \text{for } -1 \le \mu \le 0 \tag{4}$$

meaning that there is no diffuse intensity coming into the slab of random medium. $\mu = cos\theta$ is the cosine of the polar angle, 4 by 1 vector $\mathbf{F_o}$ is the source term corresponding to the incident flux magnitude and 4 by 4 matrix $\mathbf{S}$ is the Muller matrix. t is the normalized time (actual time / (L/c)) where c is the light speed in the medium. The time-dependent diffuse intensity can be calculated by applying a Fourier transform to the solution of the Eq. (3)

$$\mathbf{I}_d(t,\tau) = \frac{1}{2\pi}\int\mathbf{I}_d(\omega,\tau)\exp\left(i\frac{\omega}{\tau_o}\tau - i\omega t\right)d\omega \tag{5}$$

where $\mathbf{I}_d(t,\tau)$ is the diffused component modified Stokes vector in time-domain.

$$\mathbf{I}_d(t,\tau) = \left[I_1(t,\tau) \quad I_2(t,\tau) \quad U(t,\tau) \quad V(t,\tau)\right]^T \tag{6}$$

The total specific intensity consists of coherent (reduced) intensity and incoherent (diffuse) intensity. The coherent intensity is expressed as

$$\mathbf{I}_{ri}(t,\tau) = \mathbf{I}_o \exp(-\tau)\delta(\phi)\delta(\mu - 1)\delta(\mathrm{t - z/L}) \tag{7}$$

where $\mathbf{I}_o$ is the incident modified Stokes' parameter. We consider two cases of incident waves. For linear polarization in x direction,

$$\mathbf{I}_o = [1 \quad 0 \quad 0 \quad 0]^T \tag{8}$$

and for left-handed circular polarization,

$$\mathbf{I}_o = [1/2 \quad 1/2 \quad 0 \quad 1]^T \tag{9}$$

For incoherent intensity, we solve Eq. (1) with the boundary conditions stated in Eq. (2) using the discrete ordinates method with Gauss quadrature formulas. The discrete random medium is assumed to be dielectric spheres suspended in a homogeneous background. For the purpose of this paper, we apply the fog particles with size distribution tabulated in Table 1 in the air background. As a result, the Muller matrix can be calculated using the Mie solution[9]. For linear polarization, the co-polarized component in the forward direction is in the *x*-direction and the cross-polarized component is in the *y*-direction. On the other hand, for circular polarization, the co-polarized component in the forward direction is left-handed and the cross-polarized component is right- handed.

It is important to note that Eq. (3) is not the Fourier Transform of the conventional vector radiative transfer operation, but is modified by removing the fast varying factor $\exp(\mathrm{i}\omega\tau/\tau_0)$ which makes it stable to obtain numerical solutions. It should also be noted that Eq. (3) is applicable only to spherical scatterers. For non-spherical particles such as ice crystals, the extinction coefficient is not scalar, and depends on the polarization. Therefore, we need to replace the extinction coefficient by 4x4 extinction matrix [5],[6]. Another limitation of Eq. (3) is that it is the narrow band approximation. For ultra wide band applications, it needs to be modified to the two-frequency radiative transfer equation [1].

4. IMAGING FORMULATIONS

Imaging through discrete scattering media suffers from scattering effects of intensity leading to angular spreading. The coherent component, which gives the sharpness to the images, reduces exponentially as a function of the optical depth. On the other hand, the incoherent component, which induces the blurring of the images, increases as the waves propagate deeper in scattering media. The PSF captures this characteristic and it is a measure of the performance of an imaging system. The MTF which is a spatial Fourier Transform of PSF, represents how the different spatial frequency components are transferred through the random medium [1],[8]. The contrast represents the difference between the coherent and incoherent intensities and is a measure of how the intensity is transferred from the coherent to the incoherent components. The performance of an imaging system degrades as the optical waves encounter more scattering from the medium for the reasons given above.

We also define the degree of polarization (DOP), which is a measure of the ratio of the polarized component of the intensity to the total intensity,

$$m = \frac{\sqrt{(I_1 - I_2)^2 + U^2 + V^2}}{I_1 + I_2} \tag{10}$$

The cross-polarization discrimination (XPD) is a measure of the ratio of the co-polarized to the cross-polarlized components

$$XPD = 10\log\left[\frac{I_{co-pol}}{I_{x-pol}}\right] \tag{11}$$

Consider an imaging system shown in Fig. 5. The circular lens has diameter of *D* with the focal distance of d_i. The field at the imaging plane is given by

$$u_i(\bar{x}_i) = \frac{k^2}{(2\pi d_i)^2}\int u_o(\bar{x}) W_p(\bar{x}) \exp\left(i\frac{k}{2d_i}(\bar{x}_i^2 - 2\bar{x}_i\bar{x})\right)dx \tag{12}$$

where the pupil aperture function $W_p(\bar{x})$ is 1 for $|\bar{x}| \le D/2$ and 0 for $|\bar{x}| > D/2$. $u_o(\bar{x})$ is the incident field on the lens. The intensity at the imaging plane is

$$I_i(\bar{x}_i) = \left\langle u_i(\bar{x}_i) u_i^*(\bar{x}_i) \right\rangle = \frac{k^2}{(2\pi d_i)^2} \iint \Gamma(\bar{x}_1, \bar{x}_2) W_p(\bar{x}_1) W_p(\bar{x}_2) \exp\left(-i \frac{k}{d_i} \bar{x}_i . (\bar{x}_1 - \bar{x}_2) \right) d\bar{x}_1 d\bar{x}_2 \tag{13}$$

With $\bar{x}_c = (\bar{x}_1 + \bar{x}_2)/2$ and $\bar{x}_d = \bar{x}_1 - \bar{x}_2$, and the assumption that the Mutual Coherence Function (MCF) $\Gamma(\bar{x}_1, \bar{x}_2) = \Gamma(\bar{x}_d)$ becomes

$$I_i(\bar{x}_i) = \frac{k^2}{(2\pi d_i)^2} \iint \Gamma(\bar{x}_d) W_p(\bar{x}_1) W_p(\bar{x}_2) \exp\left(-i \frac{k}{d_i} \bar{x}_d \bar{x}_i \right) d\bar{x}_d \, d\bar{x}_c \tag{14}$$

where the MCF $\Gamma(\bar{x}_d)$ is given by

$$\Gamma(\bar{x}_d) = \int I_o(\bar{s}) \exp(ik\bar{s}\bar{x}_d) d\bar{s} \tag{15}$$

and $\bar{s} = \dfrac{\bar{x}}{d_i} = \sin\theta\cos\phi\, \hat{x} + \sin\theta\sin\phi\, \hat{y}$. The MCF consists of coherent and incoherent parts shown in the Eq. (16).

$$\begin{aligned} \Gamma_{coh}(\bar{x}_d) &= \int I_{o-coh}(\bar{s}) \exp(ik\bar{s}\bar{x}_d) d\bar{s} = \int \exp(-\tau_o) \delta(\bar{s}) \exp(ik\bar{s}\bar{x}_d) d\bar{s} = e^{-\tau_o} \\ \Gamma_{incoh}(\bar{x}_d) &= \int I_{o-inc}(\bar{s}) \exp(ik\bar{s}\bar{x}_d) d\bar{s} = \int I_d(\bar{s}) \exp(ik\bar{s}\bar{x}_d) d\bar{s} \end{aligned} \tag{16}$$

Substituting the Eq. (16) into Eq. (14), we have

$$I_i(\bar{x}_i) = I_{i-coh}(\bar{x}_i) + I_{i-inc}(\bar{x}_i) = \frac{k^2}{(2\pi d_i)^2} \left[e^{-\tau_o} A_i(k\bar{s}_i) + \int I_d(\bar{s}) A_i(k\bar{s}_i - k\bar{s}) d\bar{s} \right] \tag{17}$$

where the Airy pattern $A_i(k\bar{s}_i)$ is the point spread function of the imaging system given by

$$A_i(ks_i) = \left[\pi a^2 \frac{J_1(ks_i a)}{\frac{1}{2} ks_i a} \right]^2, \quad s_i = |\bar{s}_i| \tag{18}$$

From Eq. (17), we can conclude that the specific intensity at the imaging plane is the combination of coherent intensity and incoherent intensity. The coherent component is the Airy pattern multiplied with a factor exponentially decreased by optical depth. On the other hand, the incoherent component is the convolution of diffuse intensity incident into the lens with the Airy pattern. The Optical Transfer Function (OTF) is the spatial Fourier Transform of Eq. (17) and its magnitude is the MTF. OTF is given by

$$H(\bar{f}) = H_m(\lambda d_i \bar{f}) H_o(\lambda d_i \bar{f}) \tag{19}$$

where H_m is the normalized MCF through the random medium and H_o is the diffraction limited OTF of the lens.

$$H_m = \frac{\Gamma(\lambda d_i \bar{f})}{\Gamma(0)} \tag{20}$$

$$H_o = \begin{cases} \dfrac{2}{\pi} \left[\cos^{-1}\left(\dfrac{x_d}{D} \right) - \dfrac{x_d}{D} \left(1 - \dfrac{x_d^2}{D^2} \right)^{1/2} \right] & \text{if } x_d < \mathrm{D} \\ 0 & \text{if } x_d > \mathrm{D} \end{cases}$$

Alternatively, we can write Eq. (17) as follows:

$$I_i(\bar{s}_i) = \int \Gamma(\bar{x}_d) \frac{\pi D^2}{4} H_o(\bar{x}_d) \exp(-ik\bar{s}_i \cdot \bar{x}_d) d\bar{x}_d \tag{21}$$

where $\bar{s}_i = \bar{x}_i / d$

5. IMAGING THROUGH FOG AND CLOUDS

There have been extensive studies made on imaging through particles [9],[10]. The use of polarization and pulse has also been studied by many people [11],[12],[13]. We consider following examples. Fog particles have size distribution centered near 1 μm. The medium thickness is 1 *km*, the wavelength $\lambda = 1\,\mu m$, and the lens diameter is *D* = 1 *m*. Fig. 6 shows DOP and XPD for CW case. Note that the CP maintains its DOP for much larger optical depth than the LP. MTF, PSF, and contrast are also shown in Fig.7, 8, and 9. The cross-polarized component is mostly diffuse and the co-polarized component consists of the ballistic, minimally scattered wave, and diffuse wave.

Therefore, the difference between the Co-pol and X-pol may be mostly ballistic and minimally scattered waves, and thus the polarization differential technique may give improved image resolution. This is shown in Fig. 9.

6. PULSE IMAGING

Fig. 10 shows the pulse shape of PSF at different angles close to the optical axis. It is expected that the minimally scattered pulses do not contribute much to the improvement of the images if the particle sizes are comparable or small compared with the wavelength. The situation may be quite different if the particle sizes are much greater than the wavelength, which is usually the case for cirrus clouds. For large non-spherical ice crystal particles, the above radiative transfer solutions are not applicable. We can, however, use the equivalent circular particles and obtain the solution using the second order multiple scattering theory [14].

7. COMPARISON WITH TURBULENCE SCATTERING

Optical imaging through turbulence has been studied extensively [1],[8]. We use the same formulation given in Section 4. The mutual coherence function through turbulence is given by

$$\Gamma(\bar{x}_d) = \exp\left[-\left(\frac{x_d}{\rho_o}\right)^{5/3}\right] \tag{22}$$

where ρ_o is the coherence length and is related to Fried parameter r_o

$$\rho_o = 2.1 r_o \tag{23}$$

The coherence length ρ_o is given by

$$\rho_o = \left[1.46 k^2 C_n^2 L\right]^{-3/5} \tag{24}$$

where C_n is the structure constant. For our calculation, we use AMOS night data [8]

$$C_n^2 L = \begin{matrix} 0.6879 x 10^{-12} & (m^{1/3}) \\ 2.220 x 10^{-12} & (m^{1/3}) \end{matrix}$$

It is also known that the cross-polarization is negligible in turbulence. Fig. 11 shows PSF for particle and turbulence. Note that for turbulence, the coherent component quickly dies down and the transmitted wave is almost all incoherent wave.

8. NON-SPHERICAL PARTICLES

Vector radiative transfer equation in Eq. (3) is applicable only to spherical particles. In order to study the imaging through non-spherical particles, it is necessary to calculate the 4 by 4 Mueller matrix, which can be obtained by 2 by 2 Scattering amplitude matrix. It is also necessary to calculate the 4 by 4 Extinction matrix [5],[6]. It is, however, numerically difficult to solve the radiative transfer equation. It needs to be expanded in Fourier series in azimuthal (ϕ) direction. Unlike spherical particles, all Fourier components are coupled, creating prohibitively large matrix equations. For non-spherical particles, a simpler approach is to use the first and second order scattering solutions. Since most of the important scattering characteristics in the near-forward direction are contained in the first order scattering, this technique gives a reasonable approximation to determine the imaging with the minimally scattered (snake) waves.

9. ANGULAR AND TIME GATING

If we have an array of detectors at the image plane, we can obtain the output with the angular (ΔS) and the time (Δt) gating. For example, for the same time gating, the resolution is improved if the FOV (ΔS) is narrower. For the same FOV (ΔS), the smaller time gating reduces the incoherent intensity. This is shown in Fig. 12.

10. CONCLUSIONS

In this paper, we first reviewed the optical scattering characteristics of clouds. We then presented the time-dependent vector radiative transfer theory and summarized the definitions of Degree of Polarization (DOP), Cross-

Polarization Discrimination (XPD), and contrast. We also discussed Point Spread Function (PSF) and Modulation Transfer Function (MTF). We then presented numerical examples of imaging through clouds at $\lambda = 1\,\mu m$ and lens diameter $D = 1\,m$. Advantage of circular polarization over linear polarization is discussed in term of DOP. It is also noted that polarization differential technique may give improved resolution.

Ballistic and minimally scattered (snake) waves are discussed in terms of PSF and pulse characteristics, showing the improved image resolution for large particles. Comparison with imaging through turbulence is also discussed showing high resolution for coherent intensity in particles, and high resolution for incoherent intensity in turbulence. Some additional comments are included on the imaging through non-spherical ice crystals, showing the need for further study on first and second order vector radiative transfer.

ACKNOWLEDGEMENT

This work is supported by the Air Force Research Laboratory (F29601-00-C-0240), National Science Foundation (ECS-9908849), and Office of Naval Research (N0001400010027). We thank Dr. Charles Matson, AFRL, for many discussion, comments, and suggestions.

REFERENCES

[1] A. Ishimaru, *Wave Propagation and Scattering in Random Media*, 574 pages, IEEE Press, Piscataway, New Jersey and Oxford University Press, Oxford, England, An IEEE-OUP Classic Reissue, 1997.

[2] A. Ishimaru, "Wave Propagation," Chapter 37 in *Handbook of Applied Meteorology*, D. D. Houghton, editor, pp. 1031-1064, John Wiley and Sons, New York, 1985.

[3] G. Asrar, ed, *Theory and Application of Optical Remote Sensing*, John Wiley & Son, New York, 1989.

[4] R. T. Landesman, P. J. Kindilien, C. L. Matson, and T. R. Caudill, "Imaging transfer through Cirrus clouds," *Pre-print.*

[5] R. Cheung and A. Ishimaru, "Multiple scattering effects on wave propagation due to rain," *Annales des Telecommunications*, 35, pp. 373-379, November-December 1980.

[6] R. Cheung and A. Ishimaru, "Transmission, backscattering, and depolarization of waves in randomly distributed spherical particles," *Applied Optics*, 21:20, pp. 3792-3798, October 1982.

[7] A. Ishimaru, S. Jaruwatanadilok, and Y. Kuga, "Polarized pulse waves in random discrete scatterers," *accepted for publication in Applied Optics.*

[8] M. C. Roggemann and B. Welsh, *Imaging Through Turbulence*, CRC Press, NY, 1996

[9] N. S. Kopeika, "Aerosol modulation transfer function: an overview," *SPIE*, Vol. 3125, pp. 214-225, 1997

[10] L. R. Bissonnette, "Calculation method of the modulation transfer function in aerosol media," SPIE, Vol. 1312, pp.148-156 , 1990.

[11] S. G. Demos and R. R. Alfano, "Optical Polarization imaging," Applied Optics, Vol. 36, pp. 150-155, 1997.

[12] K. M. Yoo and R. R. Alfano, "Time resolved depolarization of multiple backscattered light from random media," *Physics Letters*. Vol. A 142, pp. 531-536, 1989.

[13] A. D. Kim, S. Jaruwatanadilok, A. Ishimaru, and Y. Kuga, "*Polarized light propagation and scattering in random media*," SPIE, Vol. 4257-A, 2001.

[14] Y. Kuga, A. Ishimaru, and Q. Ma, "The second-order multiple scattering theory for the vector radiative transfer equation," Radio Science, 24:2, pp. 247-252, March-April 1989.

Table 1. Refractive and absorption indices of water at 25°c $n = n' + in''$

Wavelength (μm)	n'	n''
0.5	1.335	0.1×10^{-8}
1	1.327	0.289×10^{-5}
5	1.325	0.0124
10	1.218	0.0508
15	1.27	0.402

Table 2. Parameters of 1 *km* fog layer in the vicinity of Point-Loma

Wavelength (μm)	Optical depth	Albedo	Mean cosine
0.5	14.830	~1.0	0.8411
1	16.760	~1.0	0.8299
10	8.837	0.6537	0.8792

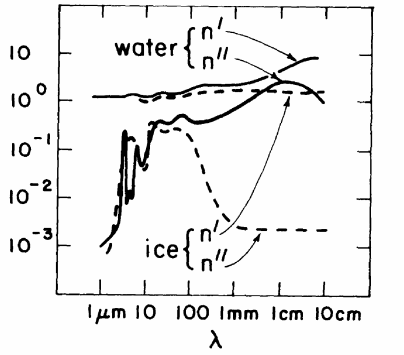

Fig. 1. Refractive index of water (10°c) and ice $n = n' + in''$

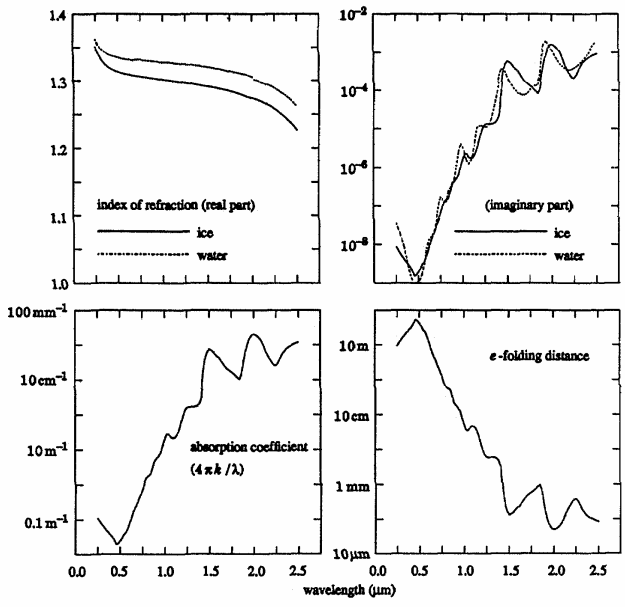

Fig. 2. Refractive indices of water and ice

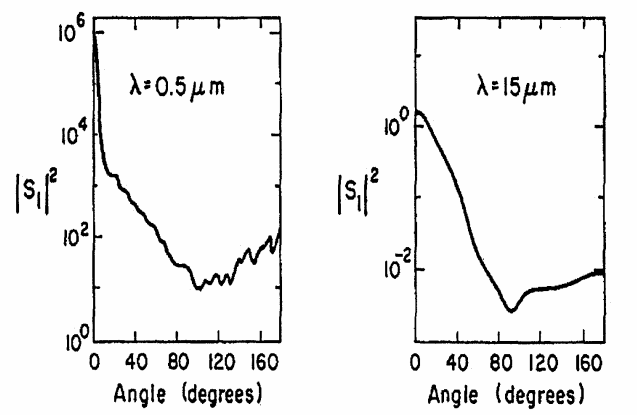

Fig. 3. Scattering pattern of fog particles

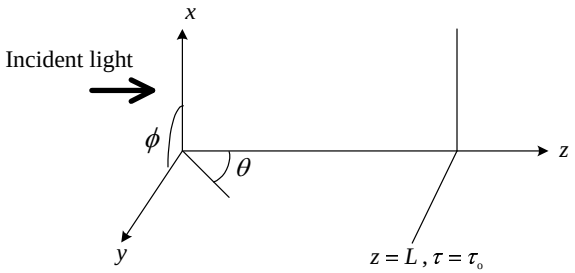

Fig. 4. Plane parallel problem

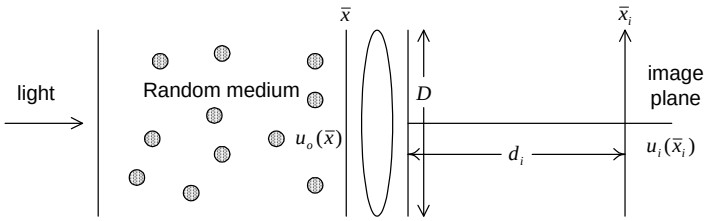

Fig. 5. Imaging system

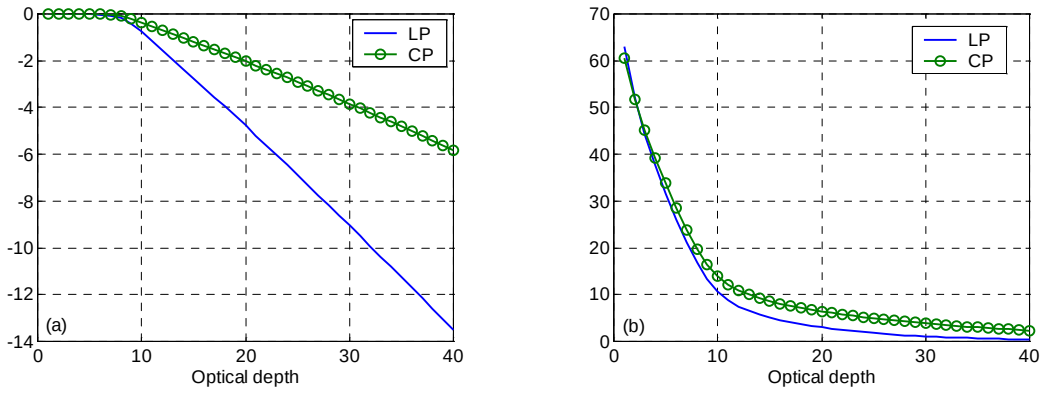

Fig. 6. a) DOP and (b) XPD in the forward direction (in decibels) as a function of optical depth

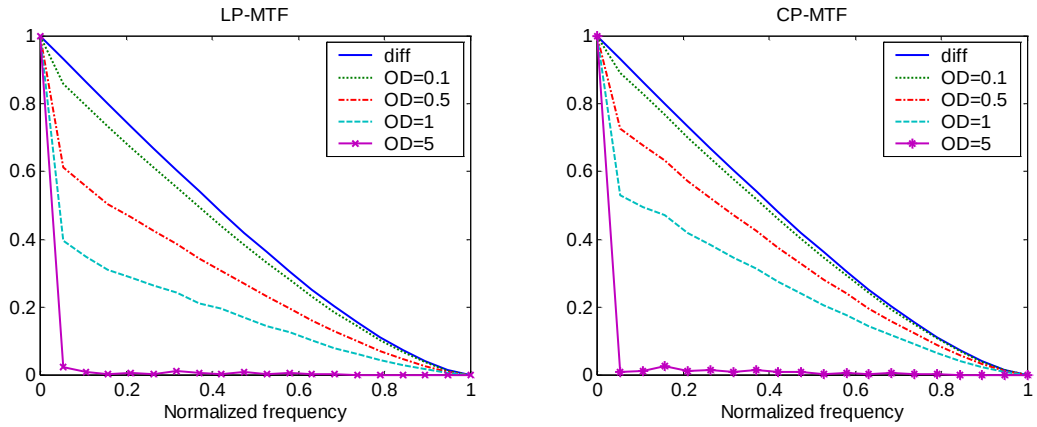

Fig. 7. MTF of Co-Pol component for CP and LP in CW case (Diff = diffraction limit, OD = Optical Depth)

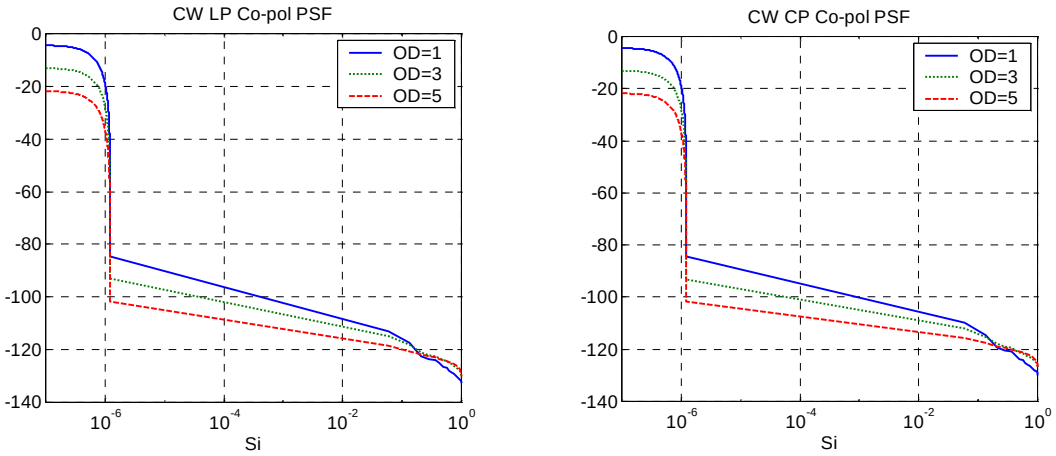

Fig. 8. PSF of Co-Pol component for CP and LP in CW case

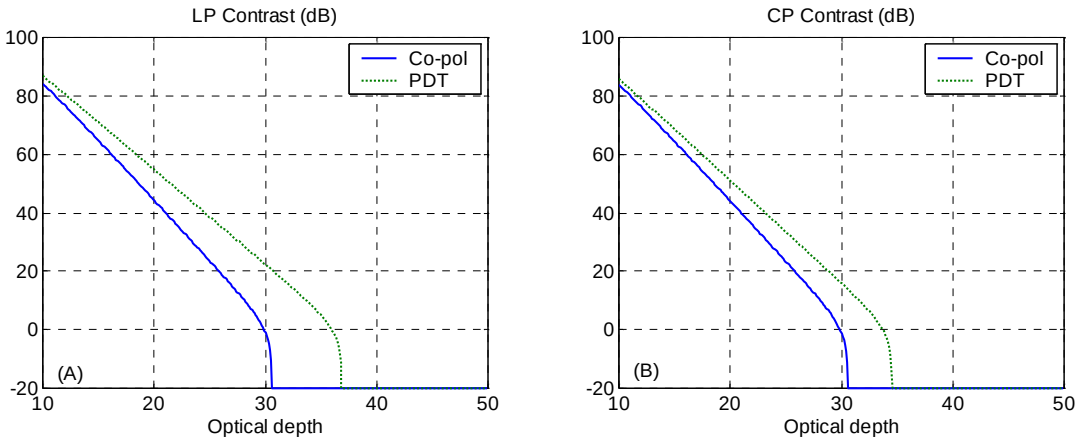

Fig. 9. Contrast (in decibel) for CW (A) LP (B) CP (PDT = Polarization Differential Technique)

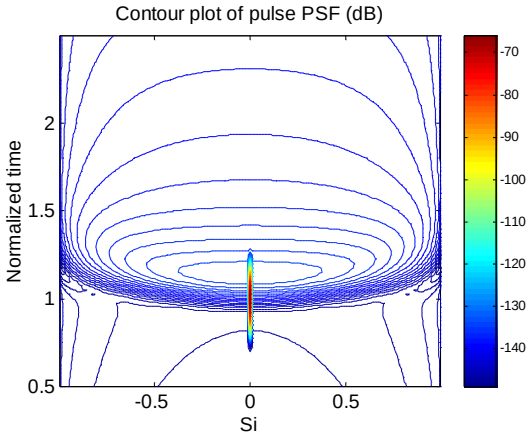

Fig. 10. Contour plot of pulse PDF (dB)

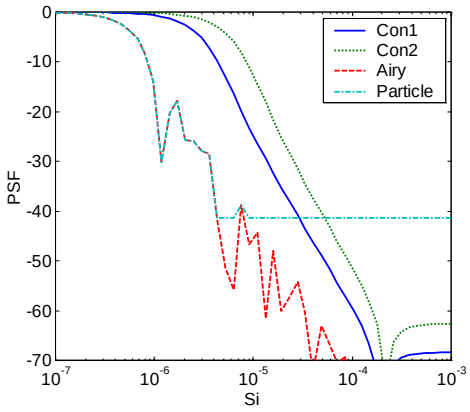

Fig. 11. PSF for particles and turbulence

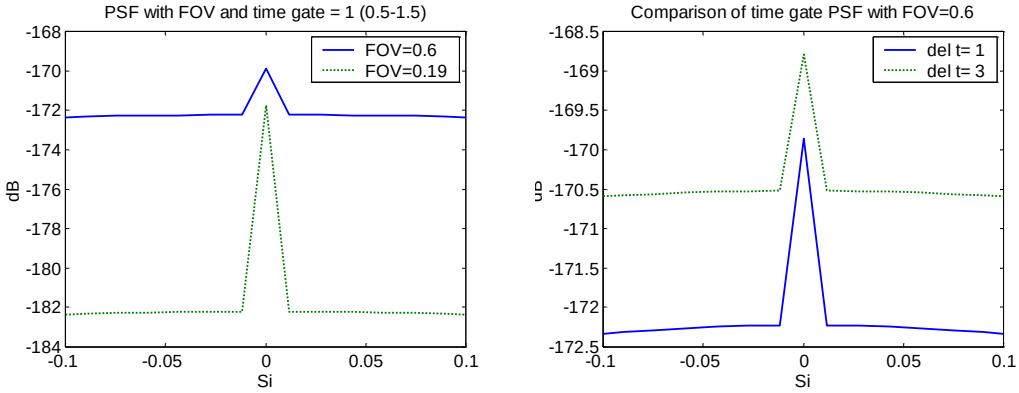

Fig. 12. Effects of FOV and time gating. Optical depth is 10